A Theoretical Study of the Land and Sea Breeze Circulation[1]

J. NEUMANN AND Y. MAHRER

Dept. of Meteorology, The Hebrew University of Jerusalem, Israel

(Manuscript received 18 January 1971)

ABSTRACT

Estoque's model for the sea breeze is modified with respect to some essential and other, less essential, details. It is shown among other things that the accelerational terms in the equation for the vertical component of motion are important and should therefore be retained. In addition, the equation of continuity is retained in its original form in order to prevent violation of the mass conservation law. The new model is integrated numerically and the results presented. The results include horizontal and vertical winds, mass conservation, vertical components of vorticity, time hodographs, temperatures (including vertical profiles), vertical transfer of sensible heat, and wind stress at the surface. Particular attention is paid to the land breeze phase of the circulation which so far has received little attention in the published literature. Further, the sea breeze front is discussed in some detail.

The integration is carried out for three daily cycles setting out from an atmosphere at rest. The results for Days 2 and 3 as well as for the second part of Day 1 are in good agreement.

1. Introduction

The nonlinear equations of the sea breeze circulation have been studied by Pearce (1955), Fisher (1961), Estoque (1961, 1962), Magata (1965) and McPherson (1970). None of these studies examines the land breeze phase of the sea and land breeze circulation (SLBC). To be strictly correct, Estoque (1961) has published one diagram relating to a night hour, but otherwise offers little comment on the dynamics of the land breeze.

Our primary concern was the study of the dynamics of the land breeze. Since Estoque's model discriminates between conditions of forced and free convection (the eddy viscosity and eddy conductivity are made functions of the Richardson number), allowance thus being made for variations in static stability, it was natural to try accomplishing our objective by first studying the predictions of Estoque's model for the land breeze. In studying his model numerically, however, we noted that it does not conserve mass to an acceptable degree of approximation. As a matter of fact, Estoque (1962, pp. 249–250) himself states: ". . . the results appear to indicate some violation of mass conservation. . . ." An illustration of the degree of violation is given in Table 1a.

Another undesirable feature of the results of computations based on Estoque's model is as follows: We carried out integrations of the model up to 48 hr, beginning with an atmosphere at rest at 0000 (relative time) on Day 1. While we did not expect, of course, that the results for the first few hours of Day 2 would agree with the corresponding values of Day 1, we did expect closer agreement between the results for, say, the second halves of Days 1 and 2. This anticipation was not fulfilled to, what we considered, a satisfactory measure and, certainly, not to the extent found in the improved model (see Fig. 6 and comments in Section 5).

We have, therefore, found it necessary to modify Estoque's model; the results with respect to both land and sea breezes are presented below.

2. Modification of Estoque's model

Estoque found that the equation of continuity, used in conjunction with the hydrostatic approximation, leads to computational instability, while the combination of the hydrostatic approximation and the vertical derivative of the equation of continuity permitted a numerically stable integration. Estoque, therefore, adopted the vertical derivative as one of the equations of his model. It is apparent that the introduction of a derivative of the equation of continuity, in lieu of the equation of continuity itself, leads to a violation of mass conservation in numerical calculations.

It will be shown presently for the SLBC that one cannot justify neglect of the vertical acceleration in the equation for the vertical component of motion. As the order of magnitude of the depth of the SLBC is 1 km and as the density varies across that depth by just under 10%, we will take the density as constant, i.e., we will base our estimates on an effectively homogeneous fluid.[2] For such a fluid we can write the equation for the

[1] Presented at the AMS–IMS International Conference on Meteorology, Israel, 30 November–4 December 1970.

[2] The homogeneous fluid approximation is only made in this section.

vertical component of motion in terms of a *modified* pressure P (see, e.g., Batchelor, 1967, p. 176), in the form

$$\frac{\partial w}{\partial t}+u\frac{\partial w}{\partial x}+\cdots+w\frac{\partial w}{\partial z}=-\frac{\partial(P/\rho)}{\partial z}, \tag{1}$$

where P arises wholly from the effect of motion. Further, the equation of continuity is

$$\frac{\partial u}{\partial x}+\cdots+\frac{\partial w}{\partial z}=0. \tag{2}$$

We let L, H, U and W be the characteristic magnitudes, respectively, of x (or y), z, u (or v) and w. Then, from (2), we have

$$\frac{U}{L}=\frac{W}{H}\left(=\frac{1}{\tau}, \text{ say}\right), \tag{3}$$

so that $L/U=(H/W)=\tau$ is the characteristic time scale of the circulation. Since U, L and H for the SLBC are, characteristically, 5 m sec^{-1}, 50 km and 1 km, respectively, W works out as 10 cm sec^{-1}. Adopting, as usual, the quantity W^2 for the characteristic scale (P/ρ), and introducing the other relevant scales, (1) becomes

$$\frac{UW}{L}+\frac{UW}{L}+\cdots+\frac{W^2}{H}=\frac{W^2}{H}.$$

With UW/L being of the same order of magnitude as W^2/H, i.e., 10^{-3} cm sec^{-2}, it is clear that we must not neglect any of the acceleration terms in the equation for the vertical component of motion, i.e., we abandon the hydrostatic approximation. Fisher's (1961) paper has the terms in question but his model does not possess many of the other attractive features of Estoque's model.

Estoque divides the atmospheric layer affected by the SLBC into two sublayers: (i) a constant-flux layer close to the surface, taken to be 50 m thick; and (ii) a transition layer of 1950 m. The equations for sublayer (i) are those involving the height-independent turbulent vertical fluxes of horizontal momentum and sensible heat (the SLBC is taken to be a "dry" system), while the usual equations of motion, continuity and heat conduction apply to sublayer (ii). Problems of numerical integration have led us to change Estoque's boundary condition for the pressure disturbance (see below). Thus, the modifications introduced by us so far relate to sublayer (ii). However, we will later introduce other changes of lesser importance.

We set out from an atmosphere at rest and assume that, initially, the meteorological variables are uniform along horizontal surfaces. Some of the other assumptions are: 1) the earth's curvature can be neglected, 2) the coastline is straight, subtending an angle ψ with north, 3) the vertical fluxes of horizontal momentum and sensible heat are due to turbulence, the eddy viscosity and conductivity being equal, and 4) the horizontal fluxes of the quantities can be neglected.

At the beginning of the integration, we impose the first two harmonics of a diurnal temperature wave at the land surface, in order to simulate the asymmetry of the surface temperature variation (Kuo, 1968, Fig. 5). The sea surface temperature is taken as constant. As a result of differential heating, motion sets in and the temperature as well as the pressure change. The components of motion and the differences between the initial values of temperature and pressure and those at any time after the onset of heating are considered as disturbance variables. We further assume that values of the disturbance variables along any horizontal line parallel with the coast are constant, i.e., their derivatives with respect to the coordinate axis parallel to the shoreline vanish.

3. Equations and boundary conditions[3]

a. Constant-flux layer: $0\leqslant z\leqslant h$

$$\frac{\partial}{\partial z}\left(K\frac{\partial U}{\partial z}\right)=0, \tag{4}$$

$$\frac{\partial}{\partial z}\left(K\frac{\partial \theta_T}{\partial z}\right)=0, \tag{5}$$

where

$$K=[k_0(z+z_0)(1+\alpha \mathrm{Ri})]^2\frac{\partial U}{\partial z}, \quad \text{for} \quad \mathrm{Ri}>-0.03, \tag{6}$$

$$K=\lambda z^2\left(\frac{g}{\bar{\theta}_T}\left|\frac{\partial \theta_T}{\partial z}\right|\right)^{\frac{1}{2}}, \quad \text{for} \quad \mathrm{Ri}\leqslant -0.03. \tag{7}$$

Following Estoque (1961), we take $\lambda=0.9$ and $z_0=1$ cm. On the other hand, we take $\alpha=-0.3$ in contrast to Estoque's value of -3. We adopted this latter value after carrying out a number of computer experiments designed to calculate the flux of sensible heat under conditions of forced convection. The calculations relate to the energy balance of the coastal plain of central Israel from which estimates of the vertical flux of sensible heat are obtained. Details of this will be published later.

b. Transition layer: $h\leqslant z\leqslant H$

The equations of motion, continuity and heat conduction are as follows:

$$\frac{\partial u}{\partial t}+u\frac{\partial u}{\partial x}+w\frac{\partial u}{\partial z}=-\frac{1}{\rho}\frac{\partial p}{\partial x}+fv+\frac{\partial}{\partial z}\left(K\frac{\partial u}{\partial z}\right), \tag{8}$$

$$\frac{\partial v}{\partial t}+u\frac{\partial v}{\partial x}+w\frac{\partial v}{\partial z}=-fu+\frac{\partial}{\partial z}\left(K\frac{\partial v}{\partial z}\right), \tag{9}$$

[3] A list of symbols is given in the appendix.

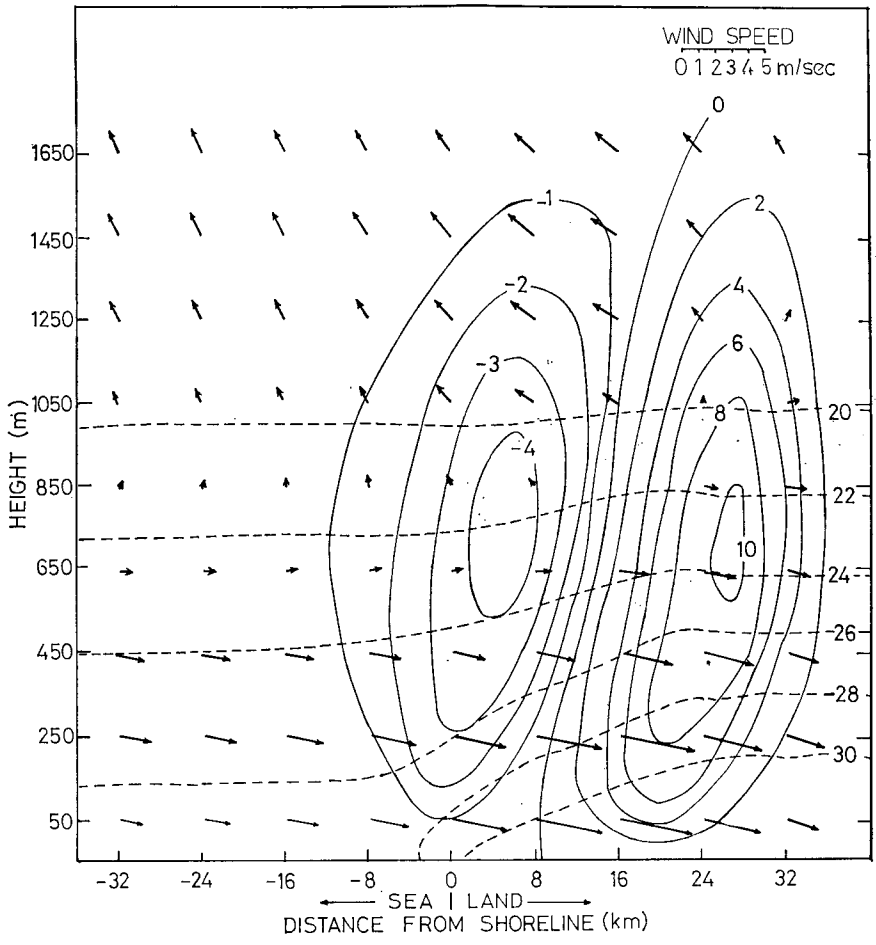

FIG. 1. Horizontal winds (m sec^{-1}, heavy arrows), vertical winds (cm sec^{-1}, thin full lines) and temperatures (°C, heavy dashed lines) for 1345 local time, Day 2. The base points of the arrows are placed at the height for which they represent the horizontal wind. For the horizontal winds north is upward and the coastline is assumed to run north-south. For a coastline forming an angle ψ with due north the arrows are to be rotated by the angle ψ. The lengths of the arrows are proportional to speed, as shown on the upper right-hand corner scale.

$$\frac{\partial w}{\partial t}+u\frac{\partial w}{\partial x}+w\frac{\partial w}{\partial z}=-\frac{1}{\rho}\frac{\partial p}{\partial z}-\frac{1}{\rho}\frac{\partial p_1}{\partial z}-g, \tag{10}$$

$$\frac{\partial u}{\partial x}+\frac{\partial w}{\partial z}=0, \tag{11}$$

$$\frac{\partial \theta}{\partial t}+u\frac{\partial \theta}{\partial x}+w\frac{\partial \theta_T}{\partial z}=\frac{\partial}{\partial z}\left(K\frac{\partial \theta_T}{\partial z}\right), \tag{12}$$

$$K=K(h)\frac{H-z}{H-h}. \tag{13}$$

The equation of state and Poisson's equation for adiabatic processes reduce the number of unknown variables to five.

c. Initial and boundary conditions

Numerical integration problems (Section 4) have led us to change some of the essential boundary conditions pertaining to Estoque's model, i.e., those relating to the pressure disturbance. Of the less essential boundary conditions we have changed the form of the temperature wave for the land surface which represents the differential heating of the land beginning at 0800 local time or 0000 hours of Day 1 of the integration.

INITIAL CONDITIONS ($t\leqslant 0$)

$$p_1(z=0)=1000 \text{ mb} \tag{14a}$$

$$T_1(z=0)\equiv\theta_1(z=0)=26\text{C} \tag{14b}$$

$$T_1(z)=26-6.5\times10^{-5}z \tag{14c}$$

BOUNDARY CONDITIONS ($t>0$)

$z=0$:

$$u=v=w=0 \tag{15a}$$

$z=0$:

$$T_T(x<0)\equiv T_1(x<0)=26\text{C}, \quad T(x<0)\equiv 0 \tag{15b}$$

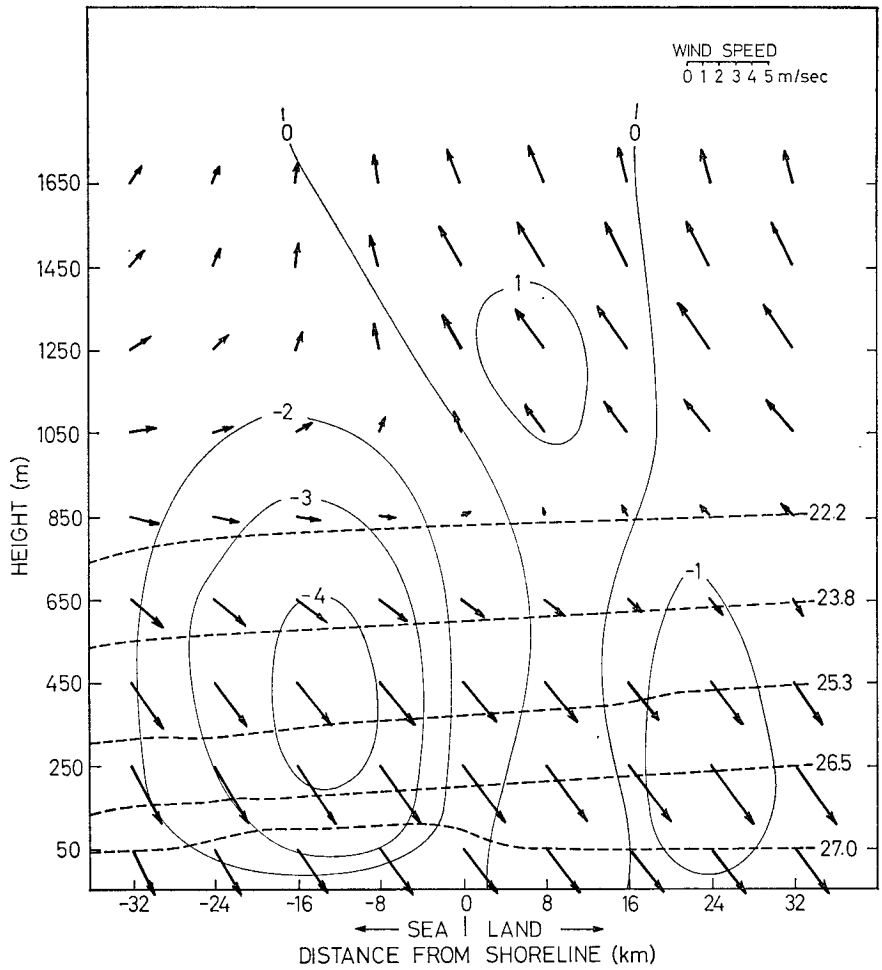

FIG. 2. Same as Fig. 1 except for 2000 local time, Day 2.

$z=0$:

$$\left.\begin{aligned} T(0<x\leqslant 20\text{ km},\, t) &= 2.8+\left(10+\frac{x}{10^6}\right)^* \\ &\quad \times\sin(15t+6)+3.4\sin(30t+310) \\ T(x>20\text{ km},\, t) &\equiv T(x=20\text{ km},\, t) \end{aligned}\right\} \quad (15c)$$

$z=0$:

$$T_T(x=0,\, t)=\tfrac{1}{2}[T_T(x<0)+T_T(x>0)] \quad (15d)$$

$z=H$:

$$u=v=w=\theta=0 \quad (15e)$$

$x=\pm L$:

$$w=p^*=0,\quad \frac{\partial}{\partial x}(u,v,\theta)=0 \quad (15f)$$

The form of the two-harmonic diurnal temperature wave for the land surface [(15c)] has been taken from Kuo's (1968, Fig. 6) paper for a soil depth of 0.5 cm. His computations are based on a radiative-convective model and compare well with observations taken in a summer season at O'Neill, Nebr., by the Great Plains Turbulence Project (Lettau and Davidson, 1957). We have reduced his curve's range to 20C as a result of the modifying effect of the nearby water surface.

In (15c) the additive term $x/10^6$ increases the amplitudes from the coast as far as 20 km inland. This rate of increase is based on conjecture and is not a firm figure. We have stopped the increase at 20 km for we noted from air temperature observations in Israel that there is little change in the air temperature range beyond about 20 km from the Mediterranean coast (excepting areas which are well above or well below mean sea level).

d. *Matching of solutions*

We followed Estoque's procedure for matching the solutions for sublayers (i) and (ii) at their interface.

4. Numerical aspects

The numerical solution of Eqs. (8)–(13) with initial and boundary conditions (14) and (15) has been greatly facilitated by a recent paper of Chorin (1968). In fact, it is his paper that prompted us to introduce the condition $p^*=0$ at the lateral boundaries in lieu of Estoque's

* x in $x/10^6$ is in centimeters.

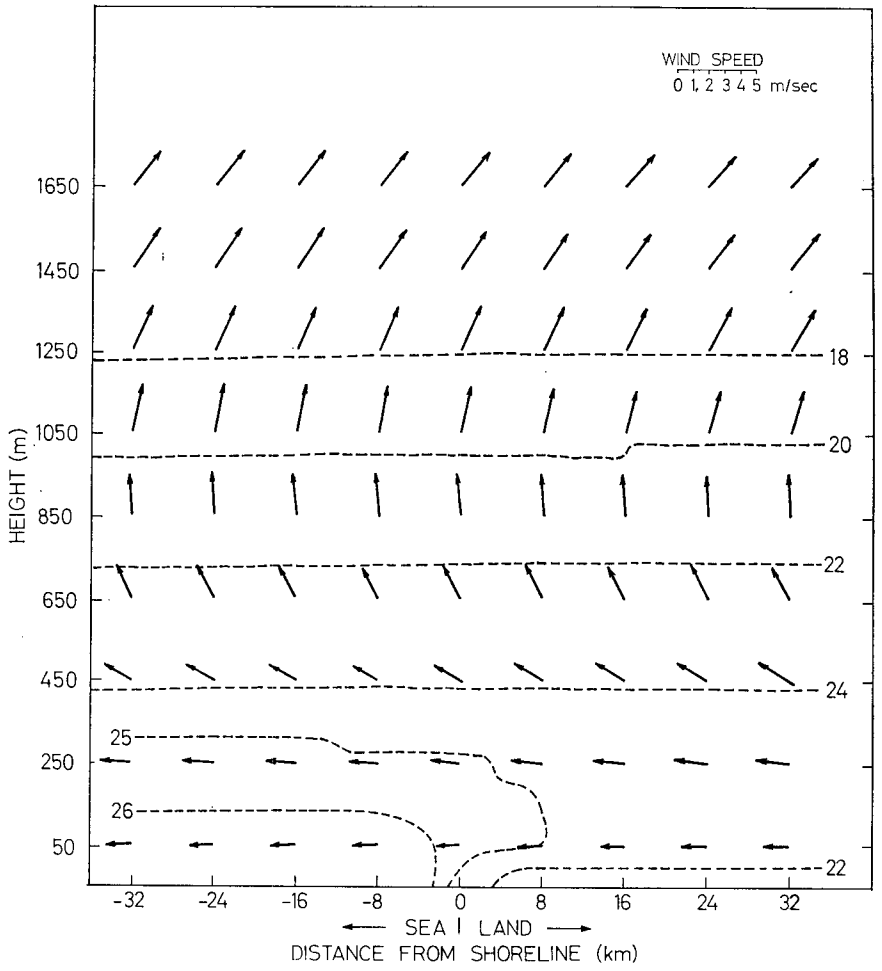

FIG. 3. Same as Fig. 1 except for 0200 local time, Day 2.

boundary condition $\partial p/\partial x=0$. Further, our model does not prescribe a boundary condition for p at $z=H$.

It will be noted that Eq. (10) for the vertical component of motion does not include the Coriolis term whose order of magnitude is similar to that of the accelerational terms. Unfortunately, we have not yet been able to devise a numerically stable scheme for the case where the term in question is retained. We hope that other investigators will succeed in finding a stable solution.

Our horizontal grid interval is 4 km, and the vertical 100 m beginning at the top of the constant-flux layer. The time step is 3 min, in approximate agreement with John's (1952) result for linear parabolic equations. Ignoring the nonlinear terms in (8) and (9), John's paper requires a time step Δt such that $\Delta t \leqslant (\Delta z)^2/2K$, Δz being the vertical grid interval.

In all our calculations we have taken the Coriolis parameter for latitude 30N.

5. Results

a. Compliance with the continuity equation

Tables 1 and 1a show for every second grid point the computed values of the velocity divergence, $(\partial u/\partial x)+(\partial w/\partial z)$, in both Estoque's model and in the present model at a time point equal to 6 hr after the beginning of integration. We find that at most hours and grid points $\partial u/\partial x$ and $\partial w/\partial z$ are of the order of 10^{-5}–10^{-4} sec^{-1}. In Estoque's model, using a numerical scheme essentially identical with his, the signs of the two terms are frequently the same. As a result the sums of the two terms are often of the same order as those of the individual terms. In our model at most grid points the sum of the two terms is of the order of 10^{-7} and less, i.e., two to three, and more, orders of magnitude smaller than the individual terms. Near the shoreline the velocity divergence is somewhat large.

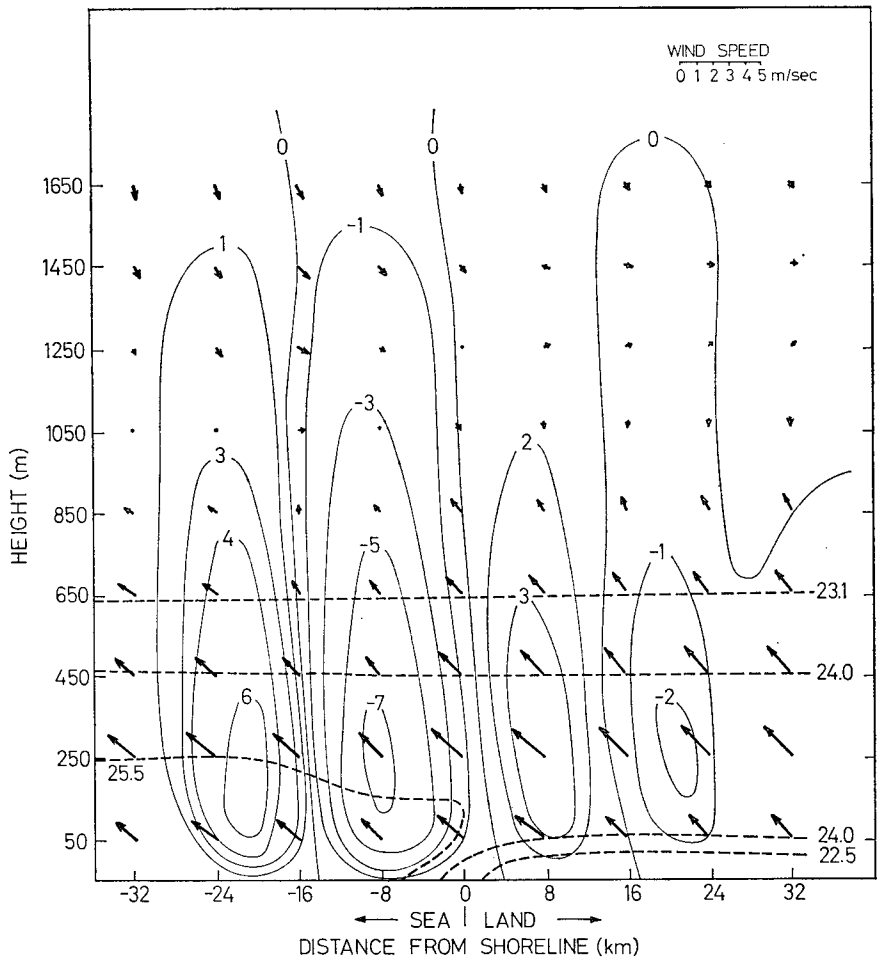

FIG. 4. Same as Fig. 1 except for 0600 local time, Day 2.

b. Horizontal winds and temperatures

Figs. 1–4 show the distributions of the computed temperatures and the horizontal and vertical components of the winds for selected hours of Day 2. It is important to note that *the arrows represent the horizontal wind* at the pertinent height, the base points of the arrows being placed at the height in question. Their direction is appropriate to a shoreline directed north-south. If the supposedly straight shoreline subtends an angle ψ with north, the arrows are to be rotated by ψ. In the case of the coast line of central Israel, for example, the shoreline forms an angle of approximately 20° clockwise from north; hence, the depicted wind directions should be made to *veer* 20° for that coastal area.

Fig. 1 refers to the time when the near-surface sea breeze is at or near its maximum. The sea breeze front is clearly seen at ~24 km inland; beyond 24 km we note a marked drop in wind speed in the layer near the surface. One expects horizontal convergence and, hence, upward motion near the front. Indeed, well-developed vertical velocity cells (isotachs of vertical velocity are marked in the figure in thin full lines) are found near the front with the largest values (10 cm sec^{-1}) occurring close to the front at heights of between 600–850 m. Particularly striking is the temperature drop behind the front if we recall that initially the isothermal surfaces were horizontal. The isothermal surface for 26C lowers nearly 300 m from its height ahead of the front to its height over the sea at the point where that surface levels off (about 8 km from the shore). The temperature decrease behind the front is noticeable to an altitude of about 1 km.

Fig. 2 is for a transition hour while Figs. 3 and 4 show the land breeze near the surface. The gradual turning of the direction of the winds in the course of the diurnal cycle is quite obvious in these diagrams. Figs. 3 and 4 also show the deepening of the land breeze layer during the second part of the night. While it is somewhat difficult to conceive of a land breeze front, cold land air near the shoreline definitely undercuts and lifts warm sea air. Moreover, there is a fairly large horizontal temperature gradient near the coast.

At 0600 local time (Fig. 4) the vertical velocity cells are again well developed. The speeds involved are

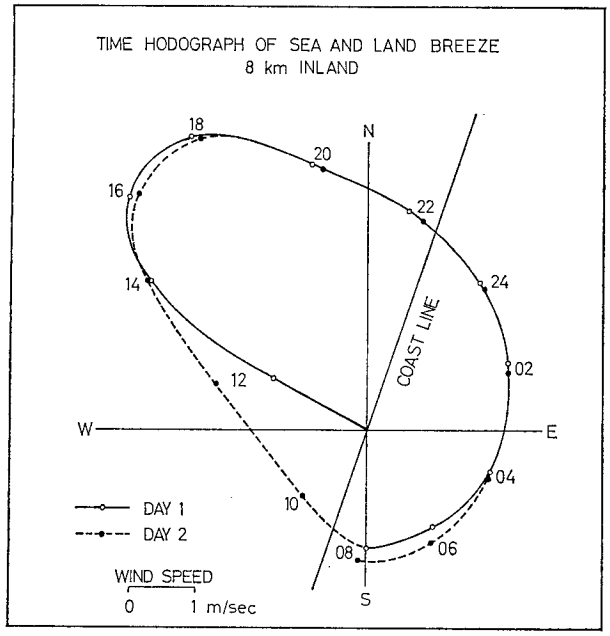

FIG. 5. In this figure the wind directions have been veered by 20° in comparison with Figs. 1–4. This rotation makes the directions correspond to the Mediterranean coast of central Israel whose direction is indicated in the diagram. The results for Day 3 are not plotted as they agree rather closely with the parallel data for Day 2. The figures along the curve are hours (local standard).

smaller and the maxima occur at lower heights than is the case for the sea breeze. Especially striking is the fact that the maximum values of vertical velocity over the land are much smaller, about one-half, than those occurring over the sea. It is plausible that the static stability of the air over the land at the time inhibits strong vertical motions. In this connection, we note in

TABLE 1. Values of $[(\partial u/\partial x)+(\partial w/\partial z)]\times 10^7$ (units, sec^{-1}) after 6 hr of integration (1400 local standard) in present model. See legend to Table 1a for definition of ordinate scale.

HEIGHT (m)									
1650	0.0	0.0	0.0	0.0	0.0	0.0	0.0	0.0	0.0
1450	0.0	0.0	0.0	0.0	0.0	0.0	0.0	0.0	0.0
1250	0.0	0.2	-0.4	0.7	0.3	-0.4	-0.6	0.2	0.0
1050	0.0	-0.1	1.3	0.7	0.8	-1.0	2.1	-0.9	0.0
850	0.0	0.2	1.5	0.8	2.6	-2.1	2.0	-1.3	0.0
650	0.0	-0.8	0.5	2.1	3.9	-4.8	-3.0	1.6	0.0
450	0.0	0.5	1.9	6.1	4.3	-5.7	-4.0	1.1	0.0
250	0.0	-0.6	1.1	-2.5	6.7	-2.1	1.8	0.2	0.1
50	0.0	1.2	0.7	-3.1	15.6	-14.3	1.0	0.6	0.1
	-32	-24	-16	-8	0	8	16	24	32

TABLE 1a. Same as Table 1 except for Estoque's model. Values along the ordinate in both tables represent distance (km) from the shoreline, with positive values over land.

HEIGHT (m)									
1650	-0.7	-4.1	-7.9	-3.2	11.0	8.1	2.3	0.1	-0.2
1450	-0.8	-4.4	-8.1	-1.8	12.0	8.2	1.5	-0.3	-0.3
1250	-0.8	-4.8	-8.3	-0.2	14.0	8.0	1.4	-0.9	-0.5
1050	-0.7	-5.4	-9.3	0.0	18.0	11.0	-5.6	-3.3	-0.5
850	-0.6	-5.6	-10.0	0.6	20.0	11.0	-1.5	-2.8	-0.4
650	-0.4	-5.5	-11.0	-1.1	27.0	19.0	-20.0	-9.5	0.0
450	-0.2	-4.9	-11.0	-3.1	22.0	18.0	-18.0	-10.0	1.3
250	0.0	-5.2	12.0	-4.0	25.0	22.0	-24.0	-20.0	0.0
50	0.4	0.1	-0.8	4.8	8.4	5.4	-13.0	-5.4	1.1
	-32	-24	-16	-8	0	8	16	24	32

both Figs. 3 and 4 the clearly indicated nocturnal temperature inversion over the land.

Although we have not treated the case of a "moist" circulation, the number of cells in Fig. 4, the usually increased relative humidities at night, and the nocturnal radiational cooling of the top of the moist lower layer suggest rather widespread cloudiness and, possibly, rows of clouds parallel with the coast at about 0600. These conjectured inferences from Fig. 4 are in relatively

TABLE 2. Vertical component of the relative vorticity (10^{-5} sec^{-1}) at 1345 local standard, Day 2, the time of the maximum development of the near-surface sea breeze. Definition of ordinate scale is given in legend of Table 1a.

HEIGHT (m)										
1850	0	0	1	0	-1	0	4	2		
1650	0	0	0	-1	-1	0	0	-1		
1450	0	0	0	0	-1	-1	-3	-1		
1250	0	0	0	0	-1	-3	-4	-2		
1050	1	1	1	0	-1	-4	-4	-1		
850	1	1	1	0	-2	-4	-4	0		
650	1	1	1	0	-2	-4	-2	1		
450	0	0	0	0	-2	-3	-1	2		
250	-1	-1	-1	-1	-1	-2	0	2		
50	-1	-1	-1	-1	-2	-1	1	2		
	-36	-28	-20	-12	-4	0 4	12	20	28	36

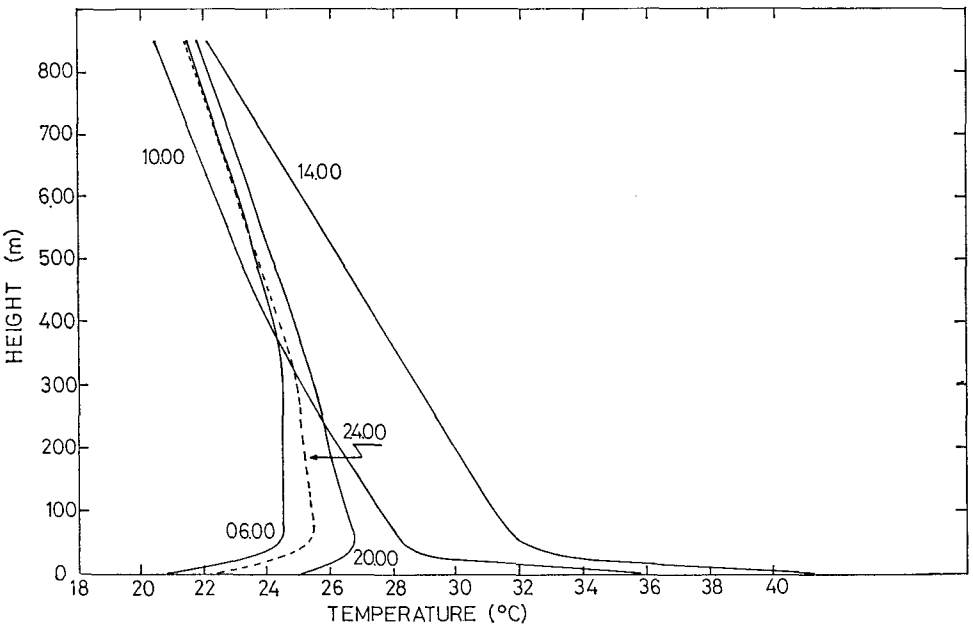

FIG. 6. Vertical profiles of temperature for five selected hours 8 km inland. The profiles for 4 km are nearly identical.

good agreement with observed conditions in the coastal area of Israel for early morning hours of the summer months.

c. *Vertical velocities, fronts and vorticity*

We have noted in Fig. 1 the relatively large values of w at 1345 local time near the sea breeze front. The order of magnitude of these velocities supports the estimates obtained in Section 2. Table 2 shows the values of the vertical component of relative vorticity, $\partial v/\partial x$, at the same time. It is seen that the largest values of relative cyclonic vorticity occur near the front.

d. *Time hodographs*

Fig. 5 is a time hodograph for a point 8 km inland. It should be noted in this diagram that the winds have been turned clockwise by 20° (relative to Figs. 1–4 and the appropriate results for other hours) in order to

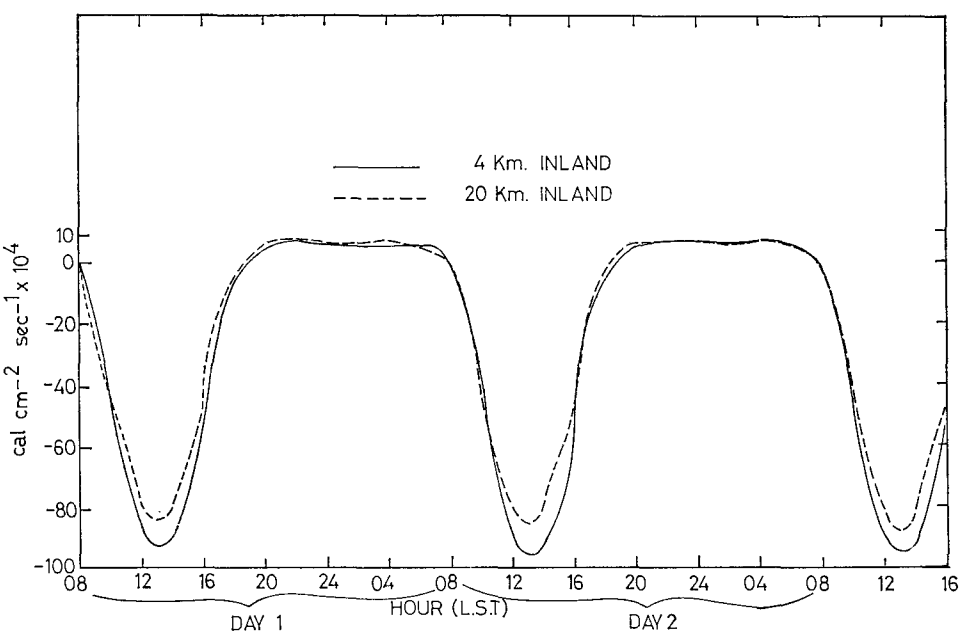

FIG. 7. Vertical transfer of sensible heat to and from the surface.

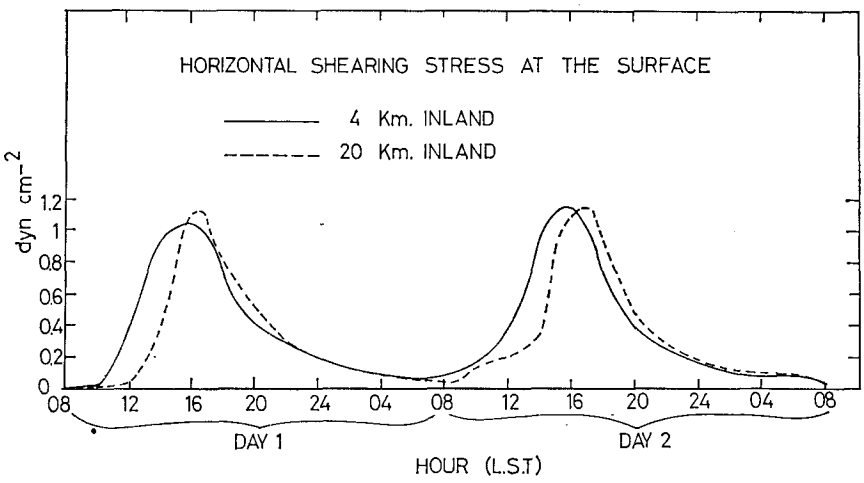

FIG. 8. Horizontal shearing stress at the surface.

conform with the direction relative to due north of the central Israel coast.

The point of major interest in this diagram is the rather close agreement between the results for the first two days beginning about 6 hr after integration. In fact, the resemblance between the results for Day 2 and Day 3 is such that it is hard to show the differences on the present scale of the diagram. We have, therefore, omitted the data for Day 3.

e. Vertical profiles of temperature

Fig. 6 shows the vertical profiles of temperature at five selected hours at a point 8 km inland. In order to form an opinion on the verisimilitude of the results, one may compare the diagram with Kuo's (1968) Fig. 1d which depicts temperature profiles measured by the Great Plains Turbulence Project at O'Neill, Nebr. (Lettau and Davidson, 1957). Though the observation hours are not quite the same, Fig. 6 appears to be reasonable. In particular, both the measurements at O'Neill and our calculations show the strong warming of the lower atmosphere in the course of the forenoon and noon hours.

f. Sensible heat transfer to and from the ground

As stated in Section 3, estimates of the energy balance for the central coastal plain of Israel in summer, including sensible heat transfer to and from the air under conditions of forced convection, have led us to adopt the value $\alpha=-0.3$ in (3). We will not discuss here the various implications of Fig. 7 as this will be done in a separate paper.

g. Horizontal shearing stress at the ground surface

Fig. 8 shows the distribution of horizontal surface shearing stress at 4 and 20 km inland. The maximum values occur shortly after the near-surface sea breeze is at its strongest and amount to $\sim$1.15–1.20 dyn cm^{-2}. The implications of Fig. 8 will also be discussed in some detail in the previously mentioned forthcoming paper.

Acknowledgments. The writers are indebted to Dr. A. Huss and Mr. E. Doron, of the Department of Meteorology, The Hebrew University of Jerusalem, for useful discussions on the subject of this paper.

APPENDIX

List of Symbols

f	Coriolis parameter
g	acceleration of gravity
h	height (50 m) of constant-flux layer
H	height (2 km) of boundary layer affected by the SLBC
k_0	von Kármán's constant
K	eddy viscosity or eddy conductivity
L	distance in the x direction of the lateral boundary of the SLBC
p	pressure
p^*	deviation of pressure from its instantaneous hydrostatic value
Ri	Richardson number
t	time
T	temperature (°C)
u, v, w	across-shore, along-shore, and vertical components of velocity
U	$(u^2+v^2)^{\frac{1}{2}}$
x, y	horizontal coordinates, respectively, perpendicular and parallel to coast
z	vertical coordinate
z_0	roughness length
α	a nondimensional constant in (6)
θ	potential temperature; $\hat{\theta}$, average potential temperature for a layer
λ	a nondimensional constant in (7)
ρ	density ($\rho\equiv\rho_T$)
ψ	angle between due north and shoreline

Subscripts

1 initial, undisturbed value
T total value, i.e., undisturbed plus disturbed values

The Finite Difference Scheme

In the numerical integration of Eqs. (8), (9), (10) and (12) the time derivatives were replaced by forward differences and the horizontal advective terms by forward differences, whenever u is negative, and by backward differences whenever u is positive.

Following Chorin (1968), the calculation of u and w from (8) and (10) is split into two steps. First, we omit the pressure gradient terms and compute the fictitious velocities u^* and w^*, respectively. Next, we re-introduce the pressure gradient terms and, using u^* and w^*, calculate u and w as follows (n is the serial number of the time step and Δt the length of the time step):

$$u^{n+1}=u^{*n+1}-\frac{\Delta t}{\rho}\left(\frac{\partial p}{\partial x}\right)^{n+1},$$

$$w^{n+1}=w^{*n+1}-\frac{\Delta t}{\rho}\left(\frac{\partial p}{\partial z}\right)^{n+1}.$$

Replacing the pressure-gradient terms by centered differences, we get the following implicit scheme:

$$u^{n+1}(I,J)=u^*(I,J)-\frac{\Delta t}{\rho(I,J)}\frac{p^{n+1}(I+1,J)-p^{n+1}(I-J,1)}{2\Delta x}, \quad (8')$$

$$w^{n+1}(I,J)=w^{*n+1}(I,J)-\frac{\Delta t}{\rho(I,J)}\frac{p^{n+1}(I,J+1)-p^{n+1}(I,J-1)}{2\Delta z}, \quad (10')$$

where $I=1, 2, \cdots, M$, $J=1, 2, \cdots, N$, I and J representing the grid points, respectively, in the x and z directions.

In difference form (11) becomes

$$\frac{u(I+1,J)-u(I-1,J)}{2\Delta x}+\frac{w(I,J+1)-w(I,J-1)}{2\Delta z}=0. \quad (11')$$

After differencing (8) and (10) with respect to x and z, respectively, and assuming

$$\rho(I+1,J)=\rho(I-1,J)=\rho(I,J+1)=\rho(I,J-1)=\rho(I,J),$$

we obtain

$$\frac{u^{n+1}(I+1,J)-u^{n+1}(I-1,J)}{2\Delta x}=\frac{u^{*n+1}(I+1,J)-u^{*n+1}(I-1,J)}{2\Delta x}-\frac{\Delta t}{\rho(I,J)}\times\frac{p^{n+1}(I+2,J)+p^{n+1}(I-2,J)-2p^{n+1}(I,J)}{4\Delta x^2}, \quad (8'')$$

$$\frac{w^{n+1}(I,J+1)-w^{n+1}(I,J-1)}{2\Delta z}=\frac{w^{*n+1}(I,J+1)-w^{*n+1}(I,J-1)}{2\Delta z}-\frac{\Delta t}{\rho(I,J)}\times\frac{p^{n+1}(I,J+2)+p^{n+1}(I,J-2)-2p^{n+1}(I,J)}{4\Delta z^2}. \quad (10'')$$

Finally, we add (8'') and (10''), and make use of the continuity equation (11'), with the result that

$$\frac{u^{*n+1}(I+1,J)-u^{*n+1}(I-1,J)}{2\Delta x}+\frac{w^{*n+1}(I,J+1)-w^{*n+1}(I,J-1)}{2\Delta z}=\frac{\Delta t}{\rho(I,J)}\left[\frac{p^{n+1}(I+2,J)+p^{n+1}(I-2,J)-2p^{n+1}(I,J)}{4\Delta x^2}+\frac{p^{n+1}(I,J+2)+p^{n+1}(I,J-2)-2p^{n+1}(I,J)}{4\Delta z^2}\right].$$

This equation is a diagnostic equation for the disturbance pressure p and is solved by an iteration process assuming (i) $u^*=u$ and $w^*=w$ on the boundaries, and (ii) a hydrostatic distribution of pressure on the lateral boundaries ($p^*=0$), i.e. (notation as in the main paper),

$$\frac{\partial p}{\partial z}=g\left(\frac{p_1}{RT_1}-\frac{p_T}{RT_T}\right).$$

The new velocity fields u^{n+1} and w^{n+1} are now calculated, respectively, from (8') and (10').

REFERENCES

Batchelor, G. K., 1967: *An Introduction to Fluid Dynamics*. Cambridge, University Press, 615 pp.

Chorin, A. J., 1968: Numerical solution of the Navier-Stokes equations. *Math. Comput.*, **22**, 745–762.

Fisher, E. L., 1961: A theoretical study of the sea breeze. *J. Meteor.*, **18**, 216–233.

Estoque, M. A., 1961: A theoretical investigation of the sea breeze. *Quart. J. Roy. Meteor. Soc.*, **87**, 136–146.

——, 1962: The sea breeze as a function of the prevailing synoptic situation. *J. Atmos. Sci.*, **19**, 244–250.

John, F., 1952: An integration of parabolic equations by difference methods. *Commun. Pure Appl. Math.*, **5**, 155–211.

Kuo, H. L., 1968: The thermal interaction between the atmosphere and the earth and propagation of diurnal temperature waves. *J. Atmos. Sci.*, **25**, 682–706.

Lettau, H. H., and B. Davidson, 1957: *Exploring the Atmosphere's First Mile*, Vol. 2. New York, Pergamon Press, 377–578.

McPherson, R. D., 1970: A numerical study of the effect of a coastal irregularity on the sea breeze. *J. Appl. Meteor*, **9**, 767–777.

Magata, M., 1965: A study of the sea breeze by numerical experimentation. *Papers Meteor. Geophys. Tokyo*, **16**, 23–36.

Pearce, R. P., 1955: The calculation of the sea breeze circulation in terms of the differential heating across the coastline. *Quart. J. Roy. Meteor. Soc.*, **81**, 351–381.